This is the accepted manuscript made available via CHORUS. The article has been published as:

Two-Dimensional Topological Insulator State in Cadmium Arsenide Thin Films

Alexander C. Lygo, Binghao Guo, Arman Rashidi, Victor Huang, Pablo Cuadros-Romero, and Susanne Stemmer

Phys. Rev. Lett. **130**, 046201 — Published 24 January 2023

DOI: 10.1103/PhysRevLett.130.046201

Two-dimensional topological insulator state in cadmium arsenide thin films

Alexander C. Lygo, Binghao Guo, Arman Rashidi, Victor Huang, Pablo Cuadros-Romero and Susanne Stemmer[a)]

Materials Department, University of California, Santa Barbara, California 93106-5050, USA

[a)] Corresponding author. Email: stemmer@mrl.ucsb.edu

Abstract

Two-dimensional topological insulators (2D TIs) are a highly desired quantum phase but few materials have demonstrated clear signatures of a 2D TI state. It has been predicted that 2D TIs can be created from thin films of three-dimensional TIs by reducing the film thickness until the surface states hybridize. Here, we employ this technique to report the first observation of a 2D TI state in epitaxial thin films of cadmium arsenide, a prototype Dirac semimetal in bulk form and a 3D TI in thin films. Using magnetotransport measurements with electrostatic gating, we observe a Landau level spectrum and quantum Hall effect that are in excellent agreement with those of an ideal 2D TI. Specifically, we observe a crossing of the zeroth Landau levels at a critical magnetic field. We show that the film thickness can be used to tune the critical magnetic field. Moreover, a larger change in film thickness causes a transition from a 2D TI to a 2D trivial insulator, just as predicted by theory. The high degree of tunability available in epitaxial cadmium arsenide heterostructures can thus be used to fine-tune the 2D TI, which is essential for future topological devices.

Two-dimensional topological insulators (2D TIs) are a highly sought-after phase owing to their spin-polarized counterpropagating (helical) edge states, which are of great interest for their ability to host novel physical phenomena, such as the quantum spin Hall effect [1-3], and for topologically protected quantum computing [4]. 2D TIs are defined as possessing an inverted (relative to a normal semiconductor band structure) and gapped band structure which together, by the bulk-boundary correspondence, give rise to $\mathbb{Z}_2$ topological order and novel edge states [1]. Despite intensive research and a number of theoretically proposed systems [5], experimentally confirmed 2D TIs are, however, very rare. Materials for which experimental signatures indicative of a 2D TI state have been reported include quantum well structures [6-8] and monolayer van der Waals compounds [9, 10].

An alternative, and largely unexplored, route to a 2D TI is thin films of three-dimensional (3D) TIs whose film thickness is reduced such that there is a spatial overlap of the surface state wavefunctions [11-13]. In this case, the 3D TI's surface states gap out, forming degenerate *massive* Dirac states, and the material is a 2D TI if there is inversion between the confinement induced electron-like and hole-like subbands [13, 14]. An additional requirement is the absence of a strong potential difference between the top and bottom surfaces of the film (so called structural inversion asymmetry or SIA) as this introduces additional coupling between the massive Dirac states that, if strong enough, destroys the 2D TI phase [13, 15, 16]. Furthermore, as a function of film thickness, it is predicted that changes in the subband ordering can cause transitions between a 2D TI and 2D trivial insulator states. The thicknesses when these transitions are expected to occur depend sensitively on band parameters and microscopic details of the system [12]. Hence, it is of interest to explore high quality thin films of 3D TIs prepared with controlled thicknesses and negligible SIA.

In this study, we employ the confinement approach to epitaxial thin films of cadmium arsenide (Cd_3As_2). While Cd_3As_2 is a prototype 3D Dirac semimetal with large band inversion in bulk [14, 17-20], it is a nearly ideal 3D TI in thin films [21, 22] with high surface state mobility and no parasitic bulk conduction at low temperature. As the Cd_3As_2 film thickness is further reduced, theory predicts a transition to a 2D TI (quantum spin Hall insulator) with a wide energy gap [14]. Recently, we reported evidence of surface state hybridization in a 20 nm-thin Cd_3As_2 thin film [23], an essential step towards a 2D TI. Here, we present the first experimental evidence of a 2D TI state in-(001)-oriented Cd_3As_2 films. To this end, we use Landau level spectroscopy, which, as we will discuss next, can unambiguously identify surface state hybridization and the inversion of the bands from the behavior of the zeroth Landau levels in high-quality films, as well as other essential details, such as SIA. Moreover, just as predicted by the theoretical models, we show that a small (6 nm) change in film thickness causes a transition from a 2D TI to a 2D trivial insulator.

A hallmark of a 2D TI in a perpendicular magnetic field (B) is a *crossing* of two zero-energy ($n = 0$) Landau levels at a critical field (B_c), as shown in Fig. 1(a), and a zero conductance ($\nu = 0$) quantum Hall plateau when the chemical potential lies in the energy gap between the $n = 0$ Landau levels (after refs. [15, 16]; for details of the calculations, see the Supplementary Materials [24]). Because of band inversion, one of the two $n = 0$ Landau levels is electron-like and originates from the valence band and the other is hole-like and originates from the conduction band. At B_c, the system undergoes a phase transition from a nontrivial insulator to a trivial one. Concurrently, the $\nu = 0$ quantum Hall plateau disappears but then reemerges for $B > B_c$. The zero energy Landau level crossing and re-entrant quantum Hall effect at B_c are robust signatures of a 2D TI state [6], while its other key feature, the helical edge states and quantum spin Hall effect, are easily obscured

by trivial edge conduction paths [27, 28] and by their extreme sensitivity to disorder [29-31]. The zeroth Landau level crossing at B_c distinguishes the 2D TI from all other potential states of a topological thin film. For example, Fig. 1 shows calculated [15, 16] Landau fan diagrams of several other possible states [24], such as the Landau level spectrum of a hybridized 3D TI *without* band inversion (a film in the trivial thickness regime, for example) [Fig. 1(b)]. Here, because band inversion is absent, all electron-like Landau levels originate from the conduction band and all hole-like ones from the valence band. Thus, the $n = 0$ Landau levels never cross and the $\nu = 0$ quantum Hall persists and widens with increasing B. If the film is in the nontrivial thickness regime but strong SIA is present, the crossing of the $n = 0$ Landau levels of the 2D TI becomes an anti-crossing [Fig. 1(c)], and the system is also a trivial insulator. Additionally, the $\nu = 0$ quantum Hall plateau is present at all B but, in contrast to the preceding case, its width evolves nonmonotonically with increasing B. Finally, Fig. 1(d) shows that a $\nu = 0$ quantum Hall state can also be observed for a *non-hybridized* (thick) 3D TI film when there is SIA and when the chemical potential lies between the $n = 0$ Landau levels of the top and bottom surfaces [32]. In this case, the $n = 0$ Landau levels are non-dispersing, as has indeed been observed for several 3D TIs [33-36], and the width of the $\nu = 0$ quantum Hall plateau is constant in B.

The presence of SIA can also be detected by characteristic crossings of Landau levels at higher energies, as seen in Figs. 1(c) and 1(d). This latter feature results in complicated filling factor (ν) sequences in the quantum Hall effect as a function of carrier density and magnetic fields, as observed for thicker (~ 50 nm) Cd_3As_2 films that are in the 3D TI state [21]. No such crossings occur without SIA [see Figs. 1(a) and 1(b)].

Combined, these distinguishing features, especially the dispersion of the $n = 0$ Landau levels and a reentrant $\nu = 0$ quantum Hall plateau, provide experimental signatures of the four

different possible phases in thin films. Clearly, it is essential to tune the Fermi level to charge neutrality and into the gap between the $n = 0$ Landau levels to distinguish these phases.

To study the electronic state of very thin Cd_3As_2 films, we performed low temperature magnetotransport measurements on top gated Hall bar structures. Details about sample growth, device fabrication, transport measurements can be found in the Supplementary Information [24]. Figures 2 (a,b) show the longitudinal (σ_{xx}) and Hall conductivity (σ_{xy}), respectively, of a 20 nm (001)-oriented Cd_3As_2 film (sample 1), calculated by tensor inversion from the resistivities (shown in the Supplementary Information [24]), as a function of applied top gate bias, V_g, and B (for a plot of V_g versus carrier density, see Supplementary Information [24]). The labels in Fig. 2(a), marking the σ_{xx} minima, denote the filling factors of the corresponding integer quantum Hall plateaus in Fig. 2(b). We observe a sequence of Landau levels that produce well defined quantum Hall plateaus with both even and odd ν. Taken alone, these filling sequences would be consistent with any of the states in Fig. 1. As discussed above, the low energy portion of the spectrum, around $\nu = 0$, is crucial to distinguish them.

We thus first turn our attention to the region around charge neutrality ($-1.5 > V_g > -2$ V). The first notable feature is the existence of a gap at zero B, as evidenced by the very low conductivity ($\sigma_{xx} \cong 0.06\ e^2/h$) and insulating behavior (the temperature dependence is discussed below). The insulating state at $B = 0$ shows that the top and bottom Dirac surface states are hybridized and, as a result, are gapped out. Moreover, the salient feature here are two Landau levels that originate at different V_g and, as B is increased, converge, meeting at approximately $B_c = 9.4$ T, before diverging for larger B. Concurrently, the $\nu = 0$ quantum Hall plateau vanishes and then remerges. This latter feature can be seen especially clearly in the σ_{xy} traces shown in Fig. 2(b): here, $\nu = 0$ is present at low B (yellow-green traces), absent at intermediate B, and reentrant

at $B > 10$ T (dark blue traces) (for additional clarity, see also the Supplementary Material for a zoom in of the σ_{xy} traces around the $\nu = 0$ plateau [24]). Accordingly, we identify the Landau levels crossing at $B_c = 9.4$ T as the $n = 0$ levels. In the regions where these two Landau levels are well separated, σ_{xx} is approximately zero and σ_{xy} plateaus at zero. By contrast, where σ_{xx} is finite (around B_c), σ_{xy} changes sign smoothly (Fig. S5 [24]). *The Landau level fan diagram is thus in perfect agreement with that of an idealized prototype 2D TI shown in Fig. 1(a).* It is *not* in agreement with either of the possible other states in Fig. 1. We note that it is the significant dispersion (in B) of both $n = 0$ levels, and the absence of any other states nearby, that allows for the clear re-entrant $\nu = 0$ quantum Hall plateau. By comparison, for HgTe quantum wells the *p*-type $n = 0$ quantum Hall plateau is nearly non-dispersive (indicative of a low Fermi velocity) and has a more complex dispersion [37, 38], causing the re-entrant quantum Hall effect to be rather complex (e.g., $\nu = 0 \rightarrow \nu = 1$ (-1) $\rightarrow \nu = 0$ [6]).

Next, we discuss the Landau level spectrum away from the charge neutrality point, important for understanding the stability of the 2D TI state in this film. There are two Landau levels, which are marked with arrows in Fig. 2(a) from a higher energy, bulk-originated subband. This is evident by the fact that they can be traced back to a different point on the V_g axis (see Fig. S6 where lines have been drawn for clarity to show the intercepts of the Landau levels with the V_g axis [24]). When the chemical potential crosses either of these additional Landau levels, ν changes by 1 [see corresponding region in Fig. 2(b)], indicating that they are non-degenerate. The existence of electronic subbands is consistent with expectations for a quantum confined thin film [12, 14].

The second important feature of the Landau level spectrum is the fact, that, with the exception of the $n = 0$ Landau levels, Landau levels that originate from the electronic states near charge neutrality do *not* cross. As discussed above, the *absence* of any other crossings in the

Landau fans to which these $n = 0$ levels belong shows that there is no perceptible energy offset (SIA), although it is present for thicker films in similar structures [21, 22]. While it is perhaps not surprising that a 20 nm thin film with a small gap does not sustain a potential offset, the absence of strong SIA is an essential pre-requisite for the observed 2D TI state. Finally, in the region $V_g <$ -2 V we observe a deep minimum in σ_{xx} and a plateau in σ_{xy} corresponding to $\nu = -1$. At more negative V_g we do not observe additional quantum Hall plateaus, possibly because the chemical potential resides in an electronic band of the buffer layer, causing spillover of carriers, or because of a high density of Landau levels from the more heavy, lower energy, valence band states (e.g., similar to HgTe quantum wells).

To demonstrate the sensitivity of the 2D TI state to small changes in film thickness, we performed additional transport measurements on 18 nm, 19 nm, and 22 nm Cd_3As films prepared under nominally identical conditions as sample 1 (see Fig. 3). The main result is a qualitatively identical Landau level spectrum. The primary quantitative differences as a function of film thickness are: (i) with increasing film thickness B_c increases, which is similar to the thickness dependence observed in HgTe quantum wells [6], and (ii) the bulk-originated subband moves to higher V_g, consist with expected behavior for quantum confined thin films. The similarity of the four Landau level spectra is in agreement with our previous observations, namely a qualitative consistency of *higher energy Landau levels* ($n > 0$) behavior with thickness [39]. However, we now see clearly the opening of a hybridization gap, which is most dramatically displayed in the behavior of the zero energy Landau levels, whose behavior extremely sensitive to the thickness.

As the film thickness is further decreased, it is predicted [14] that changes in the subband ordering cause a transition from 2D TI to a 2D trivial insulator. Figure 4 shows σ_{xx} and σ_{xy} versus V_g and B for a 14 nm film prepared under similar conditions as those discussed above.

Qualitatively, away from the charge neutrality point [Figs. 4(a) and 4(b)], the data is strikingly similar to the other samples. Quantum Hall plateaus with both even and odd ν, indicating a degeneracy lifting, are present, but no crossings of higher energy Landau levels in the low energy fans are evident, demonstrating again the absence of SIA. Distinct from the other films, the Landau levels that originate from states of a higher energy subband are absent in the V_g range studied here, consistent with the expectation that the subband ordering changes as a function of film thickness. The important difference of this film is seen near charge neutrality. For all samples, there is a clear insulating state at $B = 0$ accompanied by $\sigma_{xy} = 0$, indicating hybridization of the surface states; for the 14 nm film, however, the $n = 0$ Landau levels *diverge* and the $\nu = 0$ quantum Hall plateau widens with increasing magnetic field. The Landau level spectrum of the 14 nm film is in remarkably good agreement with that of a 2D trivial insulator shown in Fig. 1(b). We conclude from this that a 2D TI state in Cd_3As_2 can be achieved in 18-22 nm films while a small reduction in the film thickness (to 14 nm) causes a transition from a 2D topological insulator to a trivial one, consistent with the change in the subband ordering that is evident in the higher energy spectrum. Small discrepancies between the thickness ranges for the different phases in the observations vs. predictions (ref. [14]) can easily be explained by the fact the microscopic details of the heterostructures, which determine important parameters such as the Fermi velocity, were not considered in the models.

In summary, we have observed the hallmarks of a nearly ideal 2D TI state in thin films of (001)-oriented Cd_3As_2, including insulating behavior at zero field and an energy gap between two $n = 0$ Landau levels that closes at B_c. The zeroth Landau level crossing is remarkably well resolved, aided by relatively high Fermi velocities of the electronic states that give rise to the zero-energy Landau levels, low disorder, and a good separation in energy from, e.g., a high density of low

mobility valence band states found in other systems [37, 40]. These results establish that thin films of Cd_3As_2 constitute a new member of the very small, highly sought-after family of 2D TIs discovered to date. Crucially, this 2D TI state is realized via a previously theoretically suggested route, namely by quantum confinement. We also demonstrated that reducing the film thickness further induces a transition to a 2D trivial insulator, also consistent with theoretical predictions. The wide range of additional heterostructure parameters that can be tuned, such as film strain, makes the 2D TI phase in Cd_3As_2 films extraordinarily tunable. This tunability could prove extremely useful in designing and testing future superconducting hybrid junctions for quantum information systems, which depend on finely tuned energy scales, and novel correlated states [41]. This study provides clear directions for the future work such as more detailed study of the thickness dependence of the electronic state of Cd_3As_2 films, particularly one that includes ultrathin (< 10 nm) films. Finally, the results presented here demonstrate the possibility of realizing the quantum spin Hall effect in thin films of Cd_3As_2 and a next step should be investigations of the edge states physics, which requires smaller devices and low defect density mesa boundaries.

Acknowledgements

The authors are grateful to Andrea Young and Xi Dai for very helpful discussions. The research was supported by the Air Force Office of Scientific Research (Grant No. FA9550-21-1-0180) and by the Office of Naval Research (Grant No. N00014-21-1-2474). A.C.L and B.G. also thank the Graduate Research Fellowship Program of the U.S. National Science Foundation for support (Grant Nos. 1650114 and 2139319). This work made use of the MRL Shared Experimental Facilities, which are supported by the MRSEC Program of the U.S. National Science Foundation under Award No. DMR 1720256.

Appendix A: Temperature dependent conductance at ν = 0 in the 2D TI state

To further investigate the 2D TI, including the gapped state at low B, we performed temperature dependent two-point conductance (G) measurements, shown in the Supplementary Information [24]. Figure S13 [24] shows the temperature dependence of the minimum G of film 1 between the $n = 0$ Landau levels at $B < 8$ T [Fig. S13(a)], around B_c [Fig. S13(b)], and for $B > 12$ T [Fig. S13(c)]. For $B < 8$ T and $B > 12$ T, respectively, G shows an exponential-like increase with increasing temperature, consistent with a gapped state. In these two regimes, the observed temperature dependence can be described $G(T) = G_0 \exp[-(T_0/T)^p]$, where G_0 is a temperature independent prefactor, T_0 is the characteristic hopping temperature and p is a model parameter that depends on the density of states at the Fermi level and takes the values $0 < p < 1$ (see Supplementary Information [24]). A value of $p = 1$ corresponds to Arrhenius behavior and $T_0 = E_a/k_B$ where E_a is the activation energy and k_B is Boltzmann's constant. We find that for $B < 8$ T [Fig. S13(a)], the temperature dependence of G can be described by $p = 1/3$, i.e., 2D Mott variable range hopping (VRH), over some temperature range (see dashed lines). At intermediate B (7 T < B < 13 T), G shows dramatically different behavior [Fig. S13(b)]. Within this range, but away from B_c, G is a nonmonotonic function of temperature with $dG/dT > 0$ at low temperatures that transitions to T-linear dependence with a negative slope at higher temperatures. At B_c (B = 9 T and B = 10 T traces), G shows metallic behavior (it increases monotonically with decreasing temperature) and is approximately linear in temperature above 12.5 K. For $B \geq 13$ T [Fig. S13(c)], the temperature dependence roughly follows Arrhenius behavior above 3.5 K, consistent with a clean, gapped state. Most importantly, the crossover from insulating to metallic temperature dependence occurs around $B = B_c$, consistent with a *crossing* of the $n = 0$ Landau levels. Near B_c, the maximum value of σ_{xx} is ~ 0.85 e^2/h (see Supplementary Information Fig. S14 for σ_{xx} values between the $n = 0$ Landau

levels [24]). Interestingly, this σ_{xx} value is close to twice of the universal value of 0.5 e^2/h [42], consistent with the crossing of *two* Landau levels – by contrast, at the other quantum Hall transitions, σ_{xx} is close to 0.5 e^2/h. (we note that G, presented in Fig. S13, is smaller than σ_{xx}, shown, due to the contribution of contact/series resistances, including the ungated regions near the contacts). The origin of the "strange metal" (T-linear) behavior at the crossing of hole-like and electron-like zeroth Landau levels and, more generally, the nature of this "Dirac-like" state, warrants further investigations, including theoretically.

Appendix B: Detectability of the helical edge states ion the 2D TI state

We briefly comment here on the detectability of helical edge states, expected to be present for $B < B_c$. It is generally accepted in the 2D TI literature [9, 43, 44] that much smaller devices than those studied here, with carefully prepared edges [31], are needed to characterize the very fragile helical edge states, because the dimensions of the devices studied here exceed the phase coherence length (~1 μm). In devices larger than this dimension, it is generally found that σ_{xx} is smaller than $2e^2/h$ at all temperatures [9, 43, 44]. Future experiments will address fabrication challenges for smaller devices. Already in these large devices, however, the data hints at potentially rich physics. For one, the deepest minimum of σ_{xx} occurs at B = 2.4 T [σ_{xx}(2.4 T) = 0.008 e^2/h] and not at B = 0 [σ_{xx}(0 T) = 0.06 e^2/h], where the energy gap is largest (see Supplementary Information Fig. S14 [24]). This is also reflected in the temperature dependence of G, because T_0 is largest (125±8 K) at B = 2 T. One possible interpretation is that the decrease in σ_{xx} away from B = 0 reflects increased scattering of the edge states due to time-reversal symmetry breaking [45]. Competition between this enhanced scattering and the closing gap causes the minimum of σ_{xx} to occur at finite B. Secondly, VRH hopping does not completely describe the

data – at the lowest temperatures, we note that *G* saturates (see Fig. S13a), possibly indicative of a second transport path.

References

[1] C. L. Kane, and E. J. Mele, Phys. Rev. Lett. **95**, 226801 (2005).

[2] B. A. Bernevig, and S.-C. Zhang, Phys. Rev. Lett. **96**, 106802 (2006).

[3] B. A. Bernevig, T. L. Hughes, and S. C. Zhang, Science **314**, 1757 (2006).

[4] L. Fu, and C. L. Kane, Phys. Rev. Lett. **100**, 096407 (2008).

[5] C. Cao, and J.-H. Chen, Adv. Quantum Technol. **2**, 1900026 (2019).

[6] M. Konig, S. Wiedmann, C. Brune, A. Roth, H. Buhmann, L. W. Molenkamp, X. L. Qi, and S. C. Zhang, Science **318**, 766 (2007).

[7] A. Roth, C. Brune, H. Buhmann, L. W. Molenkamp, J. Maciejko, X. L. Qi, and S. C. Zhang, Science **325**, 294 (2009).

[8] L. J. Du, I. Knez, G. Sullivan, and R. R. Du, Phys. Rev. Lett. **114**, 096802 (2015).

[9] S. F. Wu, V. Fatemi, Q. D. Gibson, K. Watanabe, T. Taniguchi, R. J. Cava, and P. Jarillo-Herrero, Science **359**, 76 (2018).

[10] S. J. Tang, C. F. Zhang, D. Wong, Z. Pedramrazi, H. Z. Tsai, C. J. Jia, B. Moritz, M. Claassen, H. Ryu, S. Kahn, J. Jiang, H. Yan, M. Hashimoto, D. H. Lu, R. G. Moore, C. C. Hwang, C. Hwang, Z. Hussain, Y. L. Chen, M. M. Ugeda, Z. Liu, X. M. Xie, T. P. Devereaux, M. F. Crommie, S. K. Mo, and Z. X. Shen, Nat. Phys. **13**, 683 (2017).

[11] J. Linder, T. Yokoyama, and A. Sudbo, Phys. Rev. B **80**, 205401 (2009).

[12] H.-Z. Lu, W.-Y. Shan, W. Yao, Q. Niu, and S.-Q. Shen, Phys. Rev. B **81**, 115407 (2010).

[13] C. X. Liu, H. Zhang, B. H. Yan, X. L. Qi, T. Frauenheim, X. Dai, Z. Fang, and S. C. Zhang, Phys. Rev. B **81**, 041307 (2010).

[14] Z. J. Wang, H. M. Weng, Q. S. Wu, X. Dai, and Z. Fang, Phys. Rev. B **88**, 125427 (2013).

[15] W. Y. Shan, H. Z. Lu, and S. Q. Shen, New J. Phys. **12**, 043048 (2010).

[16] S. B. Zhang, H. Z. Lu, and S. Q. Shen, Sci. Rep. **5**, 13277 (2015).

[17] S. Borisenko, Q. Gibson, D. Evtushinsky, V. Zabolotnyy, B. Buchner, and R. J. Cava, Phys. Rev. Lett. **113**, 165109 (2014).

[18] M. Neupane, S. Y. Xu, R. Sankar, N. Alidoust, G. Bian, C. Liu, I. Belopolski, T. R. Chang, H. T. Jeng, H. Lin, A. Bansil, F. Chou, and M. Z. Hasan, Nat. Comm. **5**, 3786 (2014).

[19] Z. K. Liu, J. Jiang, B. Zhou, Z. J. Wang, Y. Zhang, H. M. Weng, D. Prabhakaran, S.-K. Mo, H. Peng, P. Dudin, T. Kim, M. Hoesch, Z. Fang, X. Dai, Z. X. Shen, D. L. Feng, Z. Hussain, and Y. L. Chen, Nat. Mater. **13**, 677 (2014).

[20] M. N. Ali, Q. Gibson, S. Jeon, B. B. Zhou, A. Yazdani, and R. J. Cava, Inorg. Chem. **53**, 4062−4067 (2014).

[21] D. A. Kealhofer, L. Galletti, T. Schumann, A. Suslov, and S. Stemmer, Phys. Rev. X **10**, 011050 (2020).

[22] D. A. Kealhofer, R. Kealhofer, D. Ohara, T. N. Pardue, and S. Stemmer, Sci. Adv. **8**, eabn4479 (2022).

[23] B. Guo, A. C. Lygo, X. Dai, and S. Stemmer, APL Mater. **10**, 091116 (2022).

[24] See Supplemental Material [link to be inserted by publisher] for the models used to calculate Fig. 1; details of the film growth, device fabrication and transport measurements; x-ray characterization of the samples; the measured resistance data from which the conductivity data shown in the main text was calculated; the gate voltage dependence of the sheet carrier density and Hall mobility extracted from the low field Hall effect; Landau level data shown in the main text with guides to the eye; the temperature dependence of G at $\nu = 0$; and the magnetic field dependence of σ_{xx} between the n = 0 Landau levels. The Supplementary Information also contains Refs. [25,26].

[25] O. F. Shoron, M. Goyal, B. H. Guo, D. A. Kealhofer, T. Schumann, and S. Stemmer, Adv. Electron. Mater. **6**, 2000676 (2020).

[26] P. Virtanen, R. Gommers, T. E. Oliphant, M. Haberland, T. Reddy, D. Cournapeau, E. Burovski, P. Peterson, W. Weckesser, J. Bright, S. J. van der Walt, M. Brett, J. Wilson, K. J. Millman, N. Mayorov, A. R. J. Nelson, E. Jones, R. Kern, E. Larson, C. J. Carey, I. Polat, Y. Feng, E. W. Moore, J. VanderPlas, D. Laxalde, J. Perktold, R. Cimrman, I. Henriksen, E. A. Quintero, C. R. Harris, A. M. Archibald, A. N. H. Ribeiro, F. Pedregosa, P. van Mulbregt, and SciPy Contributors, Nat. Methods **17**, 261 (2020).

[27] E. Y. Ma, M. R. Calvo, J. Wang, B. Lian, M. Muhlbauer, C. Brune, Y. T. Cui, K. J. Lai, W. Kundhikanjana, Y. L. Yang, M. Baenninger, M. Konig, C. Ames, H. Buhmann, P. Leubner, L. W. Molenkamp, S. C. Zhang, D. Goldhaber-Gordon, M. A. Kelly, and Z. X. Shen, Nat. Comm. **6**, 7252 (2015).

[28] F. Nichele, H. J. Suominen, M. Kjaergaard, C. M. Marcus, E. Sajadi, J. A. Folk, F. M. Qu, A. J. A. Beukman, F. K. de Vries, J. van Veen, S. Nadj-Perge, L. P. Kouwenhoven, B. M. Nguyen, A. A. Kiselev, W. Yi, M. Sokolich, M. J. Manfra, E. M. Spanton, and K. A. Moler, New J. Phys. **18**, 083005 (2016).

[29] J. Maciejko, X. L. Qi, and S. C. Zhang, Phys. Rev. B **82**, 155310 (2010).

[30] G. Tkachov, and E. M. Hankiewicz, Phys. Rev. Lett. **104**, 166803 (2010).

[31] K. Bendias, S. Shamim, O. Herrmann, A. Budewitz, P. Shekhar, P. Leubner, J. Kleinlein, E. Bocquillon, H. Buhmann, and L. W. Molenkamp, Nano Lett. **18**, 4831 (2018).

[32] T. Morimoto, A. Furusaki, and N. Nagaosa, Phys. Rev. Lett. **114**, 146803 (2015).

[33] R. Yoshimi, A. Tsukazaki, Y. Kozuka, J. Falson, K. S. Takahashi, J. G. Checkelsky, N. Nagaosa, M. Kawasaki, and Y. Tokura, Nat. Commun. **6**, 6627 (2015).

[34] Y. Xu, I. Miotkowski, and Y. P. Chen, Nat. Comm. **7**, 11434 (2016).

[35] S. K. Chong, K. B. Han, T. D. Sparks, and V. V. Deshpande, Phys. Rev. Lett. **123**, 036804 (2019).

[36] J. Ziegler, D. A. Kozlov, N. N. Mikhailov, S. Dvoretsky, and D. Weiss, Phys. Rev. Res. **2**, 033003 (2020).

[37] S. Shamim, P. Shekhar, W. Beugeling, J. Böttcher, A. Budewitz, J.-B. Mayer, L. Lunczer, E. M. Hankiewicz, H. Buhmann, and L. W. Molenkamp, Nat. Comm. **13**, 2682 (2022).

[38] W. Beugeling, Phys. Rev. B **104**, 115428 (2021).

[39] D. A. Kealhofer, M. Goyal, T. N. Pardue, and S. Stemmer, Phys. Rev. B **104**, 035435 (2021).

[40] A. M. Kadykov, S. S. Krishtopenko, B. Jouault, W. Desrat, W. Knap, S. Ruffenach, C. Consejo, J. Torres, S. V. Morozov, N. N. Mikhailov, S. A. Dvoretskii, and F. Teppe, Phys. Rev. Lett. **120**, 086401 (2018).

[41] Y. Zeng, F. Xue, and A. H. MacDonald, Phys. Rev. B **105**, 125102 (2022).

[42] S. S. Murzin, and A. G. M. Jansen, Physica E **43**, 1576 (2011).

[43] L. Lunczer, P. Leubner, M. Endres, V. L. Müller, C. Brüne, H. Buhmann, and L. W. Molenkamp, Phys. Rev. Lett. **123**, 047701 (2019).

[44] G. M. Gusev, Z. D. Kvon, E. B. Olshanetsky, and N. N. Mikhailov, Solid State Comm. **302**, 113701 (2019).

[45] P. Delplace, J. Li, and M. Buttiker, Phys. Rev. Lett. **109**, 246803 (2012).

Figure Captions

Figure 1: Characteristic Landau level spectra of different topological phases in thin films. (a) 2D TI, (b) 2D trivial insulator, (c) hybridized 3D TI with SIA, and (d) 3D TI with SIA. The labels denote quantum Hall filling factors. In (a), (b) and (c) electron-like (hole-like) levels are show in orange (blue) and in (d) Landau levels from the higher energy surface are shown in purple and those from the other surface are shown in green. In all, the $n = 0$ Landau levels are drawn with heavier line weight. All four phases can produce a $\nu = 0$ quantum Hall state (a 3D TI without SIA has degenerate $n = 0$ Landau levels and there is no $\nu = 0$ quantum Hall state). See Supplementary Materials for details of the calculations.

Figure 2: Landau levels and quantum Hall effect of sample 1 (20 nm film). Magnetic field (B) and gate voltage (V_g) dependence of the (a) longitudinal (σ_{xx}) and (b) Hall (σ_{xy}) conductivities of sample 1. The labels in (a) denote the corresponding quantum Hall filling factors in (b). The black arrows mark additional Landau levels from a higher energy subband.

Figure 3: Magnetic field (B) and gate voltage (V_g) dependence of the longitudinal (σ_{xx}) conductivity of (a) 18 nm, (b) 19 nm, and (c) 22 nm films.

Figure 4: Landau levels and quantum Hall effect of a 14 nm film. Shown are the B and V_g dependence of σ_{xx} (a) and σ_{xy} (b) of sample. Labels in (a) denote quantum Hall filling factors obtained from (b).

Figures with captions

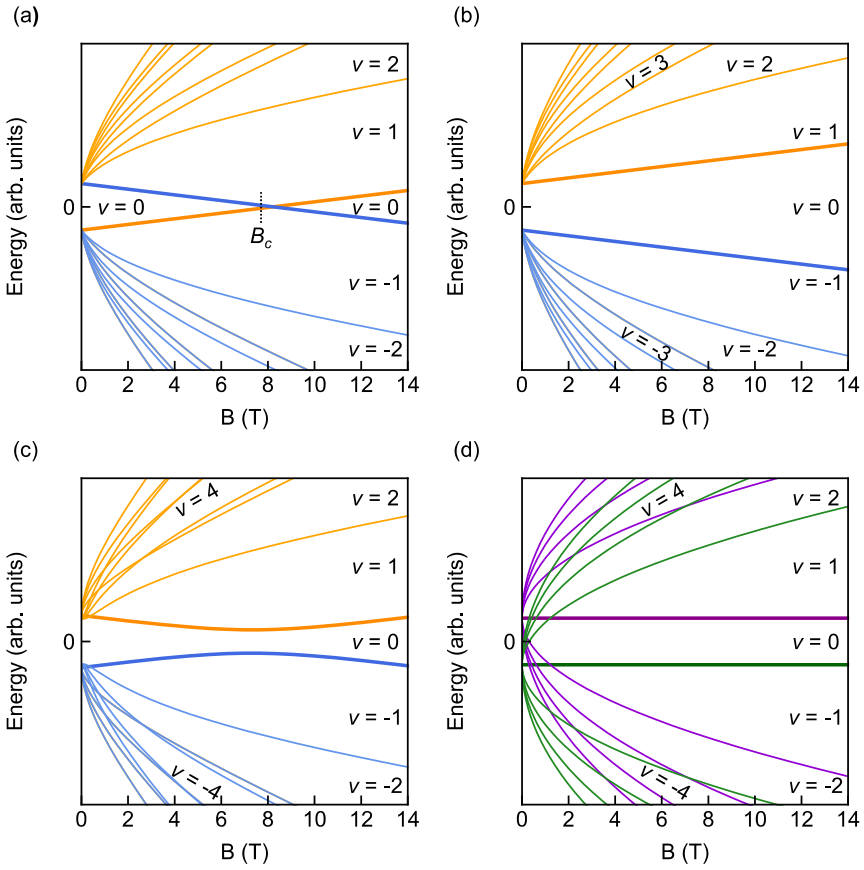

Figure 1: Characteristic Landau level spectra of different topological phases in thin films. (a) 2D TI, (b) 2D trivial insulator, (c) hybridized 3D TI with SIA, and (d) 3D TI with SIA. The labels denote quantum Hall filling factors. In (a), (b) and (c) electron-like (hole-like) levels are show in orange (blue) and in (d) Landau levels from the higher energy surface are shown in purple and those from the other surface are shown in green. In all, the $n = 0$ Landau levels are drawn with heavier line weight. All four phases can produce a $\nu = 0$ quantum Hall state (a 3D TI without SIA has degenerate $n = 0$ Landau levels and there is no $\nu = 0$ quantum Hall state). See Supplementary Information for details of the calculations.

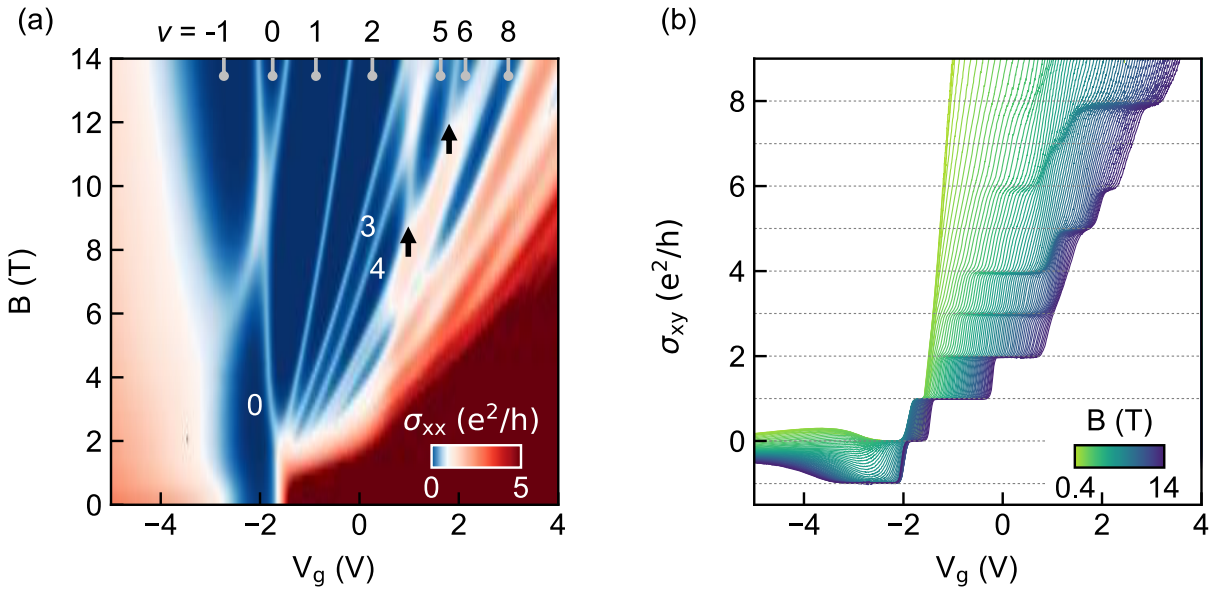

Figure 2: Landau levels and quantum Hall effect of sample 1 (20 nm film). Magnetic field (B) and gate voltage (V_g) dependence of the (a) longitudinal (σ_{xx}) and (b) Hall (σ_{xy}) conductivities of sample 1. The labels in (a) denote the corresponding quantum Hall filling factors in (b). The black arrows mark additional Landau levels from a higher energy subband.

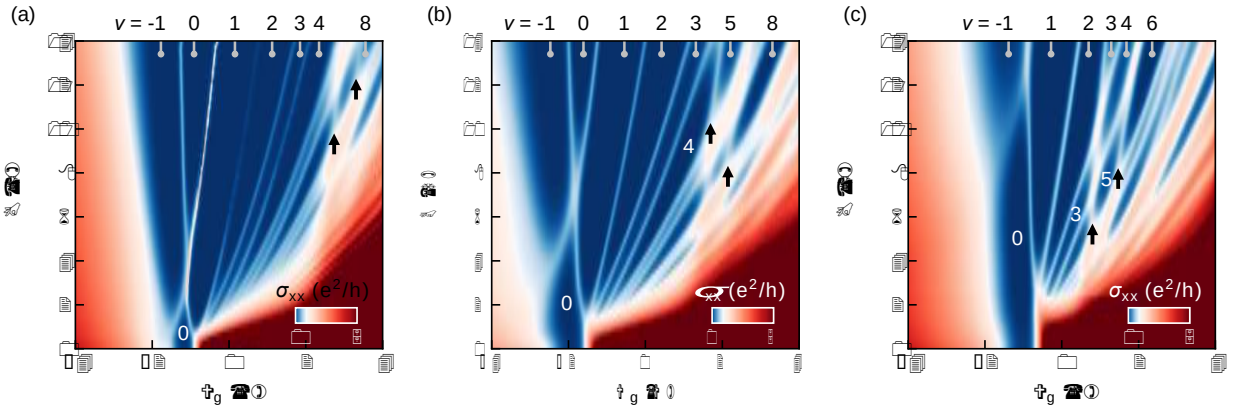

Figure 3: Magnetic field (B) and gate voltage (V_g) dependence of the longitudinal (σ_{xx}) conductivity of (a) 18 nm, (b) 19 nm, and (c) 22 nm films.

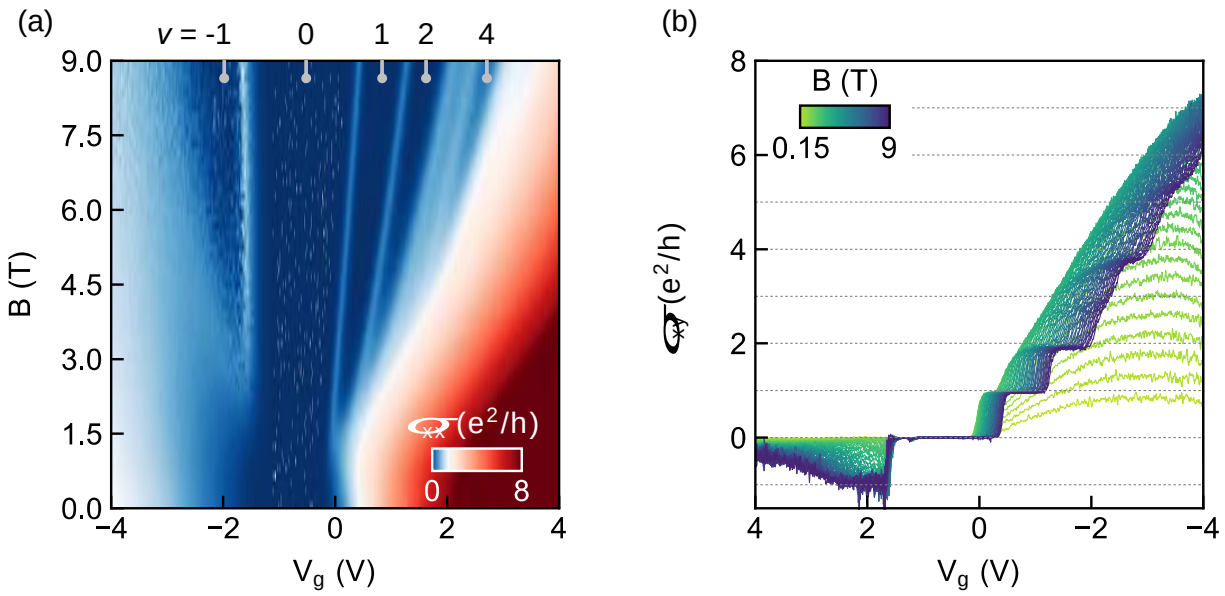

Figure 4: Landau levels and quantum Hall effect of a 14 nm film. Shown are the *B* and V_g dependence of σ_{xx} (a) and σ_{xy} (b) of sample. Labels in (a) denote quantum Hall filling factors obtained from (b).